Volume 55
Number 1
6 January 2026
Pages 1-524

Dalton Transactions

An international journal of inorganic chemistry

rsc.li/dalton

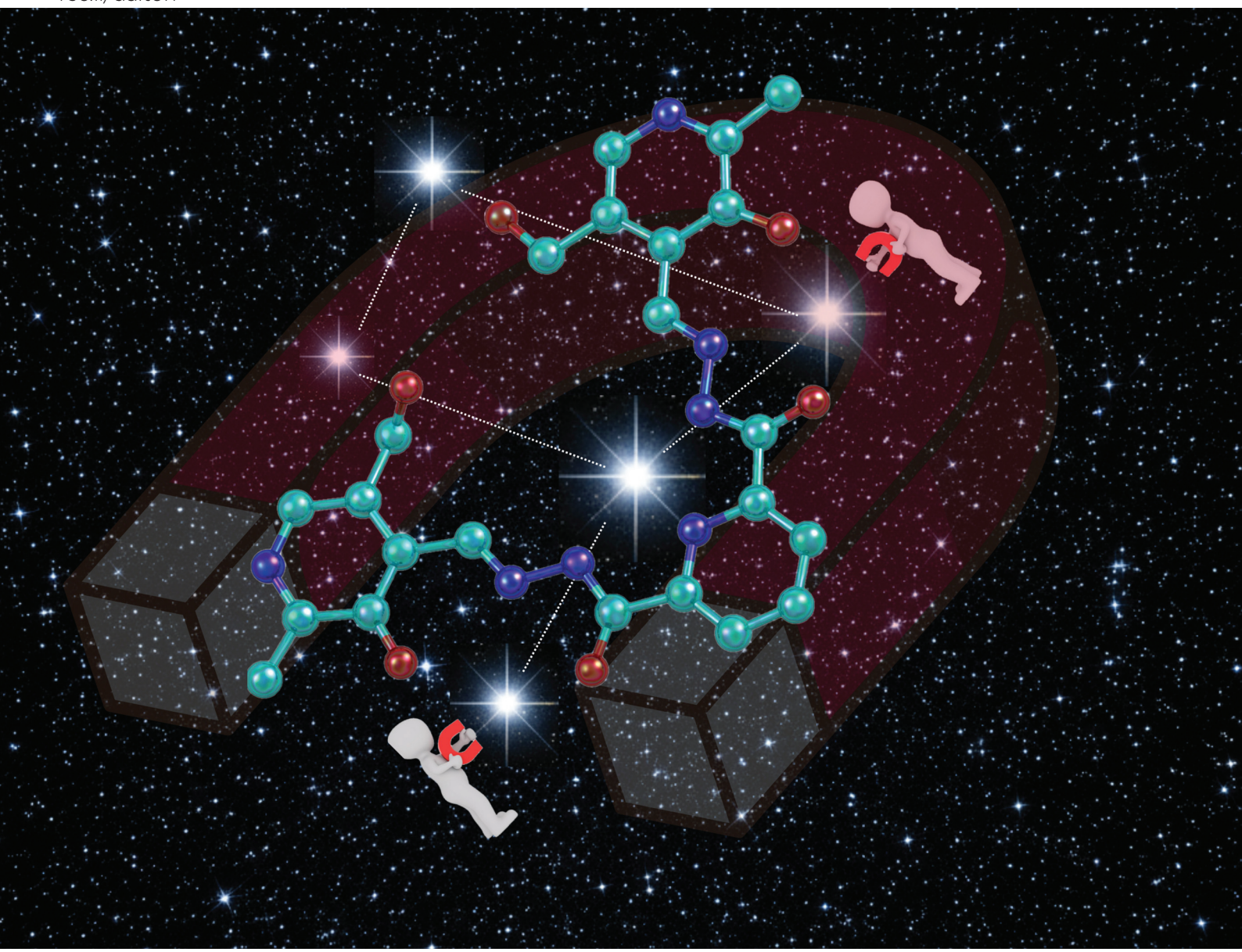

ISSN 1477-9226

PAPER

Jeremy M. Rawson, Ahmed Al-Harrasi, Muhammad U. Anwar *et al.*
Nickel and copper complexes of a new multidentate ligand: synthesis, characterization and magneto-structural investigations

ROYAL SOCIETY OF CHEMISTRY

Dalton Transactions

ROYAL SOCIETY OF CHEMISTRY

PAPER

View Article Online
View Journal | View Issue

Cite this: *Dalton Trans.*, 2026, **55**, 114

Nickel and copper complexes of a new multidentate ligand: synthesis, characterization and magneto-structural investigations

Wajid Ali,[a] Hamed Bakhshi,[b] Abdul Jabbar,[a] Melanie Pilkington,[b] Jeremy M. Rawson,*[c] Ahmed Al-Harrasi*[a] and Muhammad U. Anwar*[a]

Received 17th September 2025,
Accepted 20th November 2025

DOI: 10.1039/d5dt02226f

rsc.li/dalton

The ligand $\mathbf{L}H_8Cl_2$ ($\mathbf{L}H_6{\cdot}2HCl$) [(3-hydroxy-5-(hydroxymethyl)-2-methylpyridin-4-yl)methylene)]pyridine-2,6-dicarbohydrazide dichloride] was prepared from the Schiff base condensation of pyridine-2,6-dicarbohydrazide with pyridoxal hydrochloride in methanol. Reaction of $\mathbf{L}H_6{\cdot}2HCl$ with $CuCl_2{\cdot}4H_2O$ or $Cu(ClO_4)_2{\cdot}6H_2O$ in a MeOH/water mixture produced two 1-D copper coordination polymers with formulae $\{[Cu_3(\mathbf{L}H_4)Cl_3(H_2O)]Cl{\cdot}H_2O\}_n$ (**1**) and $\{[Cu_3(\mathbf{L}H_4)Cl(H_2O)_2(ClO_4)][ClO_4]_2{\cdot}2H_2O\}_n$ (**2**) respectively. Similarly, reaction of $\mathbf{L}H_6{\cdot}2HCl$ with $NiCl_2{\cdot}6H_2O$, $Ni(ClO_4)_2{\cdot}4H_2O$ or $Ni(NO_3)_2{\cdot}6H_2O$ afforded the trimetallic complex $[Ni_3(\mathbf{L}H_4)(H_2O)_9]Cl_4{\cdot}4H_2O$ (**3**), the 1-D polymer $\{[Ni_3(\mathbf{L}H_4)(NO_3)(H_2O)_6](NO_3)_2{\cdot}H_2O\}_n$ (**4**) and $[Ni_2(\mathbf{L}H_6)(H_2O)_6](ClO_4)_4{\cdot}3H_2O$ (**5**). The crystal structures of **1–5** were determined by X-ray diffraction. All complexes **1–4** exhibit the same geometric arrangement of the ligand with the central metal linked to the terminal metal ions by a *trans*-diazine linker with the diazine and pyridoxal arms coordinating in a tridentate NO_2 donor fashion, while the central metal atom is coordinated by the ligand in a tridentate fashion by the pyridine and two diazine-N atoms. Water and coordinating anions complete the coordination environment around the Cu^{2+} and Ni^{2+} ions. The ligand adopts the same geometry in **5** but is not deprotonated and does not possess a central metal atom. Magnetic measurements (5–300 K) reflect strong antiferromagnetic exchange across the 1,2-diazine bridge.

Introduction

Coordination chemists employ diverse strategies for constructing metallo-supramolecular architectures.[1,2] Key factors such as temperature, pH, template ions, solvent, and counter-ions significantly affect self-assembly and crystallization.[3] A prominent approach in ligand design involves the use of precisely engineered ligands featuring well-defined binding sites, paired with metal ions exhibiting complementary coordination geometries, to achieve predictable self-assembly.[4–6] This approach has yielded polydentate ligands with linear binding arrays, facilitating the rational synthesis of grids, polyhedra,[4] and extended frameworks.[7–9] Conversely, a more exploratory approach leverages serendipity, employing ligands with versatile binding modes and conformationally flexible metal ions to yield unexpected architectures.[10–12] Through systematic variation of bridge angles and ligand spacers, researchers have elucidated fundamental correlations between molecular structure and exchange coupling, advancing the understanding of these systems.[13] These principles underpin the design of polynuclear high-spin complexes, including single-molecule magnets that exhibit magnetic hysteresis at molecular scales.[14,15] Among the transition metals, copper(II) and nickel(II) complexes stand out as highly versatile systems, owing to their stable oxidation states, flexible coordination environments, and rich magnetic properties.[16–18] The magnetic properties of such systems are governed by superexchange interactions mediated by bridging ligands, with the magnitude and sign of coupling constants (J) depending critically on metal–ligand bond angles, distances, and the nature of the bridging moieties.[3] Moreover, the magnetic properties can be systematically tuned through careful design of coordination geometry and bridging ligands, enabling predictable access to antiferromagnetic, ferromagnetic, or frustrated spin states.[19] In this context, nitrogen-rich bridging ligands capable of mediating strong magnetic exchange have receive much interest. Diazine (–N=N–) bridges, in particular, have attracted attention due to their ability to transmit strong coupling between metal centers, as demonstrated in polynuclear complexes.[4] A key

[a]*Natural and Medical Sciences Research Centre, University of Nizwa, Nizwa 616, Oman. E-mail: aharrasi@unizwa.edu.om, usman.anwar@unizwa.edu.om*
[b]*Department of Chemistry, Brock University, 1812 Sir Isaac Brock Way, St Catharines, ON, L2S3A1, Canada*
[c]*Department of Chemistry and Biochemistry, University of Windsor, Canada. E-mail: jmrawson@uwindsor.ca*

challenge lies in designing ligands that can simultaneously support high nuclearity, structural dimensionality, and tunable magnetic exchange.

Pyridoxal based ligands have been largely overlooked in coordination chemistry despite their chelating capability.[20] Notably, only a few pyridoxal–diazine based ligands have been identified for the synthesis of metal complexes.[21] We hypothesized that combining these features could yield structurally robust ligand designs with polydentate pockets capable of supporting robust intramolecular magnetic exchange *via* the diazine linker.

We recently reported the complexation reactions of lanthanide salts with a tridentate diazine-based ligand ($\mathbf{LH_3}$·HCl, Scheme 1), which formed a series of lanthanide complexes.[21] In all examples, the ligand's phenolic –OH group is deprotonated and coordinates to the lanthanide metal center, while the $-CH_2OH$ group remains uncoordinated, reflecting the greater acidity of the phenol moiety. Herein, we present a new Ligand $\mathbf{LH_6}$·2HCl (Scheme 2) that combines the same tritopic bis-picolyl hydrazone core as $\mathbf{LH_3}$ with peripheral pyridoxal end groups. Ligands with the central dihydrazone core have been shown to produce numerous square grid complexes and clusters. For example, tritopic bis-picolyl hydrazones bearing pyridyl groups have resulted in $\{M_9\}$ (3 × 3) grid structures for a diversity of 3d metals (M = Fe, Co, Mn),[22] and trinuclear lanthanide complexes.[23] Similarly with phenolic end groups, the ligand afforded trinuclear copper and manganese complexes.[24] In this paper, we report a family of di- and tri-nuclear complexes and chains derived from $\mathbf{LH_6}$·2HCl. The ligand $\mathbf{LH_6}$·2HCl offers the potential to generate multiple five- and six-membered chelate rings that are well-suited to the size of typical first-row transition-metal ions. Moreover, the combination of both diazine N–N and bridging-O linkers within the structure are expected to facilitate effective magnetic communication between the transition-metal ions. In addition, the presence of the CH_2OH group on the pendant arms has the potential to coordinate further to form extended networks. In this paper we explore the reactivity of $\mathbf{LH_6}$·2HCl towards Cu^{2+} and Ni^{2+} ions and show that the ligand exhibits a robust coordination motif but the final outcome of the reaction is sensitive to the nature of the counter-anions present. Specifically, we have isolated two 1-D copper polymers (**1–2**), a trinuclear nickel complex (**3**), a 1-D nickel polymer (**4**) and a dinuclear nickel complex (**5**). The structures of **1–5** were analyzed by single-crystal X-ray diffraction. DC magnetic susceptibility data are also presented.

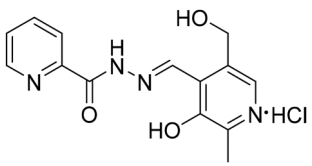

Scheme 1 Structure of $\mathbf{LH_3}$·HCl.

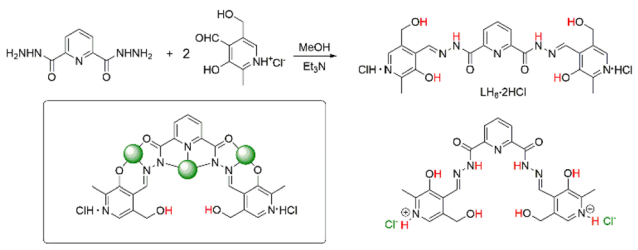

Scheme 2 Synthesis of the ligand LH_6·2HCl with two tautomeric forms shown right (potential protic H atoms on the ligand highlighted in red). Highlighted (left), the two *N,O,O′*- and *N,N′,N″*-tridentate coordination pockets of the ligand.

Experimental

Commercially available solvents and chemicals were used without further purification. Caution! Perchlorate salts are potentially explosive and should be handled with care. All reactions involving perchlorates were carried out in small quantities either behind a protective shield or using a face shield.

Physical measurements

NMR spectra were recorded on a Bruker 600 MHz spectrometer, IR spectra were obtained using a Bruker Alpha FT-IR spectrometer equipped with a Platinum single reflection Diamond ATR module. Elemental compositions were determined on a PerkinElmer 2400 Series II Elemental Analyzer. Variable temperature magnetic data (2–300 K) were obtained using a Quantum Design MPMS5S SQUID magnetometer using a field strength of 0.1 T. Polycrystalline samples were optically screened and a random selection of crystals from each batch examined by unit cell determination to check phase purity. Background corrections for the sample holder assembly and diamagnetic components of the complexes were applied.

X-ray crystallography

Table S1 provides a summary of the crystal data of complexes **1–5**. Data for complexes **1–5** were collected from a single crystal at 296(2) K and examined on a Bruker D8 Venture APEX diffractometer equipped with Photon II 14 area detector at 296 (2) K using graphite-monochromated Mo-K_α radiation (λ = 0.71073 Å). All data were integrated with SAINT V8.41.[25] A multi-scan absorption correction using SADABS 2016/2 was applied.[26] The structure was solved by intrinsic phasing methods with SHELXT 2018/2 and refined by full-matrix least-squares methods against F^2 using SHELXL-2019/2.[27,28] All non-hydrogen atoms were refined with anisotropic displacement parameters. All hydrogen atoms were refined with isotropic displacement parameters. Some of their coordinates were refined freely and some on calculated positions using a riding model with their U_{iso} values constrained to 1.5 times the U_{eq} of their pivot atoms for terminal sp^3 carbon atoms and 1.2 times for all other carbon atoms. Crystallographic data for the

structures reported in this paper have been deposited with the Cambridge Crystallographic Data Centre.[29] CCDC 2488451–2488455 contain the supplementary crystallographic data for this paper. This report and the CIF file were generated using FinalCif.[30] The powder X-ray diffraction (PXRD) scan was performed using a Bruker D8 Discover instrument operated at 40 kV with 2θ ranging from 5 to 50 (Fig. S5–S7).

Ligand and complex synthesis

Synthesis of ligand LH_6·2HCl. Pyridoxal hydrochloride (1.0 g, 4.90 mmol) was dissolved in methanol (50 mL), followed by the dropwise addition of triethylamine (0.447 mL, 3.2 mmol) under stirring. A separate solution of pyridine-2,6-dicarbohydrazide (0.396 g, 2.03 mmol)[4] in a minimal volume of methanol was prepared and added dropwise to the above reaction mixture. The resulting solution was then maintained at reflux for 24 hours, yielding a yellow precipitate. The reaction mixture was cooled and the product was collected by filtration and washed with a methanol/water mixture. The product was dried in air (Yield: 1.1 g, 1.9 mmol, 96%). Selected IR data (ν_{max}, cm^{-1}): 2981 (s), 2865 (m), 2360 (s), 1670 (s), 1522 (s), 1033 (s), 844 (w), 743, 679 (m). ^{1}H NMR (600 MHz, DMSO-d_6) δ 12.83 (s, 2H), 12.19 (s, 2H), 9.12 (s, 2H), 8.39 (d, 2H), 8.31–8.34 (dd, 1H), 7.98 (S, 2H), 5.47 (s, 2H), 4.68 (d, 4H), 2.42 (s, 6H) ^{13}C NMR (151 MHz, DMSO-d_6) δ1.59.93, 150.84, 147.89, 147.68, 147.62, 140.29, 136.68, 132.65, 126.31, 120.33, 58.94, 18.89. HRMS: calculated for $[C_{23}H_{24}N_7O_6]^+$: 494.1788, found: 494.1781.

Synthesis of complexes 1–5

*Preparation of $\{[Cu_3(LH_4)Cl_3(H_2O)]Cl{\cdot}4H_2O\}_n$ (**1**).* A mixture of $CuCl_2{\cdot}2H_2O$ (0.293 mmol, 0.05 g) and ligand LH_6·2HCl (0.10 mmol, 0.05 g) were dissolved in a 1 : 1 methanol/water mixture (20 mL total volume, 10 mL each). The reaction mixture was stirred at 60 °C for 1 hour to ensure complete dissolution, then filtered warm to remove particulates. The filtrate was allowed to cool slowly to room temperature and then left undisturbed. After three weeks, dark green crystals suitable for X-ray diffraction formed *via* slow evaporation. Yield: 0.057 g, 60%; Selected IR data (ν_{max}, cm^{-1}): 3523–3346 ($\nu_{OH/NH}$), 1625 ($\nu_{C=O}$), 1550 ($\nu_{C=N}$), 1390 (ν_{C-C}), 1056 (ν_{C-OH}). Elemental analysis calc. for $[Cu_3(C_{23}H_{21}N_7O_6)Cl_4(H_2O)]{\cdot}4H_2O$: C 30.22, H 3.42, N 10.73; found: C 30.13, H 3.74, N 10.69.

*Preparation of $\{[Cu_3(LH_4)Cl(H_2O)_2](ClO_4)_3{\cdot}2H_2O\}_n$ (**2**).* Cu $(ClO_4)_2{\cdot}6H_2O$ (0.30 mmol, 0.11 g) and ligand LH_6·2HCl (0.10 mmol, 0.05 g) were stirred at 60 °C in a 1 : 1 methanol/water solvent system (20 mL total volume, 10 mL each). The reaction mixture was the filtered and left undisturbed for crystallization at room temperature. Dark green crystals appeared after three weeks. The crystals were very hygroscopic. Yield: 0.094 g, 43%. Selected IR data (ν, cm^{-1}): 3691–3209 ($\nu_{OH/NH}$), 1658 ($\nu_{C=O}$), 1606 ($\nu_{C=C}$), 1458 ($\nu_{C=N}$), 1396 (ν_{C-C}), 1056 (ν_{C-OH}). Elemental analysis calc. for $[Cu_3(C_{23}H_{24}N_7O_6)Cl(H_2O)_2](ClO_4)_3{\cdot}10H_2O$ C 22.37, H 3.92, N 7.94; found: C 22.53, H 5.92, N 6.67.

*Preparation of $[Ni_3(LH_4)(H_2O)_9]Cl_4{\cdot}4H_2O$ (**3**).* $NiCl_2{\cdot}6H_2O$ (0.30 mmol, 0.10 g) and ligand LH_6·2HCl (0.10 mmol, 0.049 g), and triethylamine (2 drops) were stirred together in methanol (20 mL) at room temperature for 2 hours. The reaction mixture was then filtered and left undisturbed for crystallization at room temperature. Brown crystals appeared after two weeks. Yield: 0.050 g, 48%; selected IR data (ν_{max}, cm^{-1}): 3691–3215 ($\nu_{OH/NH}$), 1631 ($\nu_{C=O}$), 1537 ($\nu_{C=N}$), 1382–1245 (ν_{C-C}), 1064 (ν_{C-OH}). Elemental analysis calc. for $[Ni_3(C_{23}H_{23}N_7O_6)(H_2O)_9]Cl_4{\cdot}H_2O$: C 28.97, H 4.83, N 9.22; found: C 25.95, H 4.365, N 8.18.

*Preparation of $\{[Ni_3(LH_4)(NO_3)(H_2O)_6](NO_3)_2{\cdot}H_2O\}_n$ (**4**).* Ni $(NO_3)_2{\cdot}6H_2O$ (0.40 mmol, 0.12 g) and ligand LH_6·2HCl (0.10 mmol, 0.049 g), and triethylamine (3 drops) were stirred together in a methanol : butanol mixture (10 mL each) at room temperature for 30 min. The reaction mixture was the filtered and left undisturbed for crystallization at room temperature. Brown crystals appeared after two weeks. Yield: 0.11 g, 80%. Selected IR data (ν_{max}, cm^{-1}): 3996–3215 ($\nu_{NH/OH}$), 1631 ($\nu_{C=O}$), 1537 ($\nu_{C=O}$), 1382–1245 (ν_{C-C}), 1064 (ν_{C-OH}). Elemental analysis calc. for $[Ni_3(C_{23}H_{23}N_7O_6)(NO_3)(H_2O)_6](NO_3)_2{\cdot}4H_2O$: C 26.67, H 4.18, N 13.52; found: C 26.63, H 4.30, N 13.57.

*Preparation of $[Ni_2(LH_6)(H_2O)_6](ClO_4)_4{\cdot}3H_2O$ (**5**).* Ni $(ClO_4)_2{\cdot}4H_2O$ (0.404 mmol, 0.12 g) and ligand LH_6·2HCl (0.10 mmol, 0.049 g) were stirred at 60 °C in methanol (20 mL). The reaction mixture was the filtered and left undisturbed for crystallization at room temperature. Dark green crystals appeared after three weeks. Yield: 0.061 g, 42%. Selected IR data (ν_{max}, cm^{-1}): 3614–3240 ($\nu_{OH/NH}$), 1625 ($\nu_{C=O}$), 1543 ($\nu_{C=O}$), 1384–1242 (ν_{C-C}), 1070 (ν_{C-OH}). Elemental analysis calculated for $[Ni_2C_{23}H_{23}N_7O_6(ClO_4)_4(H_2O)_9]{\cdot}H_2O$: C 22.89, H 3.76, N 8.12; found: C 22.98, H 3.522, N 8.18.

Results

Ligand synthesis

The ligand LH_8Cl_2 (LH_6·2HCl) was prepared *via* direct condensation of pyridine-2,6-dicarbohydrazide with pyridoxal hydrochloride in methanol (Scheme 1). Addition of sufficient triethyl amine to achieve pH = 7, led to a color change to yellow and the resultant pale yellow precipitate of ligand LH_6·2HCl was isolated by filtration and washed with methanol. The structure of this new ligand LH_6·2HCl was confirmed by ^{1}H and ^{13}C NMR (Fig. S1 & S2) and HRMS. The peripheral pyridine functionalities associated with the pyridoxal group are both protonated pyridinium ions and the ligand is isolated as its hydrochloride salt. There are multiple tautomeric forms of this complex. The coordination complexes of Cu(II) and Ni(II) described here, indicate that the lower tautomeric form (Scheme 1) is a useful representation of the ligand with eight ionizable protons (red), comprising two phenolic protons, two protons associated with the hydrazine group, two protons associated with the hydroxymethyl functional group and two pyridinium protons.

Complex syntheses

Reactions of ligand LH_6·2HCl with CuX_2 (X = Cl, ClO_4) in a MeOH/water mixture produced two 1-D copper coordination

polymers with formulae $\{[Cu_3(\mathbf{L}H_4)Cl_3(H_2O)]Cl{\cdot}H_2O\}_n$ (**1**) and $\{[Cu_3(\mathbf{L}H_4)Cl(H_2O)_2][ClO_4]_3{\cdot}2H_2O\}_n$ (**2**) respectively. In the synthesis of compounds **3** and **4**, a precipitate initially formed but the addition of a few drops of triethylamine facilitated dissolution of this precipitate. The molecular structures of both complexes were determined by X-ray diffraction. For **1**, elemental analysis data suggest a total of three lattice waters per formula unit, one of which was directly located in the crystallographic study (*vide infra*) which also revealed a void space sufficiently large to accommodate up to another 3.5 water molecules per formula unit. For complex **2**, the coordinated chloride arises from the ligand which was reacted in the form of its hydrochloride salt. In a similar fashion, reaction of $\mathbf{L}H_6{\cdot}2HCl$ with NiX_2 (X = Cl, NO_3) affords the trinuclear nickel complexes $[Ni_3(\mathbf{L}H_4)(H_2O)_9]Cl_4{\cdot}4H_2O$ (**3**) and $\{[Ni_3(\mathbf{L}H_4)(NO_3)(H_2O)_6](NO_3)_3{\cdot}H_2O\}_n$ (**4**), whereas when X = ClO_4, the dinuclear complex $[Ni_2(\mathbf{L}H_6)(H_2O)_6](ClO_4)_4{\cdot}3H_2O$ (**5**) is isolated, despite the availability of excess $Ni(ClO_4)_2{\cdot}4H_2O$ (4 : 1 stoichiometry). These three Ni(II) complexes were also characterized by single-crystal X-ray diffraction, elemental analysis and IR spectroscopy.

FT-IR spectral analysis

The presence of functional and coordination behavior of important functional groups in the ligand and complexes, such as carbonyl (–C═O), imine (–C═N), and aliphatic and aromatic hydroxyl (C–OH, Ar–OH), was confirmed by FTIR spectral analysis. The peaks in the range 3200 and 3700 cm^{-1} suggest the presence of O–H stretching vibrations of coordinated and/or lattice methanol and water molecules in complexes **1–5**.[31] The –C═O stretching frequencies observed in the free ligands at 1670 cm^{-1} shifted to 1625–1631 cm^{-1} upon complexation. Similarly, the –C═N stretching frequency 1522 cm^{-1} in free ligand shifted to 1537–1550 cm^{-1} upon complexation, indicating coordination with metal ions.[32] Additionally, the medium-intensity bands of aromatic –OH observed at 1033 cm^{-1} in the free ligand was shifted to 1054–1064 cm^{-1}, suggesting deprotonation and subsequent coordination to the metal center, consistent with previous reports on structurally related ligands.[21]

Crystallographic studies

Single crystals were grown directly from the mother liquor. The crystals of complex **2** proved slightly hygroscopic, absorbing small quantities of water upon standing, but otherwise all complexes appeared to be air stable.

$\{[Cu_3(LH_4)Cl_3(H_2O)]Cl{\cdot}4H_2O\}_n$ (1). Single crystals of **1** were grown by slow evaporation of the MeOH/H_2O solution at room temperature. The complex crystalizes in the triclinic space group *P*1. Selected bond lengths and angles are listed in Table S2. In complex **1**, there are three crystallographically independent Cu sites (Fig. 1). Cu1 adopts a 5-coordinate CuN_3Cl_2 coordination geometry in which ligand LH_4^{2-} is a tridentate N3 donor. The coordination environment around Cu1 is clearly intermediate between square pyramidal and trigonal bipyramidal (observed Addison parameter[33] τ_5 = 0.47, *c.f.* τ_5 = 0.0 for square pyramidal and τ_5 = 1.0 for trigonal bipyramidal). From a trigonal bipyramidal perspective, the ligand acts as a tridentate nitrogen donor, with N atoms adopting the two apical and one equatorial position, with Cu–N bond distances ranging from 1.94(1) Å to 2.04(1) Å. Chlorine atoms Cl1 and Cl2 adopt the two remaining equatorial positions with Cu–Cl distances of 2.322(3) and 2.360(4) Å. The N–Cu–N angle between the two apical N atoms is 156.5(4)° and the sum of the three angles in the equatorial plane is 359.9°. Cu2 adopts a square pyramidal geometry (τ_5 = 0.03), with one chloride ion (Cl3) and an N_2O donor set from ligand $\mathbf{L}H_4^{2-}$ forming the basal plane and an oxygen (O_2) of another $[Cu_3(LH_4)Cl_3(H_2O)]Cl$ unit adopting the apical position. The Cu2–Cl3 distance is 2.236(5) Å. The Cu2–O distances in the basal plane are 1.904(9) and 2.002(9) Å, comparable with typical Cu–O covalent bonds (1.98 Å),[34] while the axial Cu2–O2 (CH_2OH) is substantially longer at 2.72(1) Å (ref. 29) close to the sum of the van der Waals radii (2.92 Å).[35] Cu3 adopts a square planar coordination geometry with ligand $\mathbf{L}H_4^{2-}$ offering an NO_2 donor set and the fourth coordination site taken up by a water molecule. The sum of the four angles at Cu3 is 360.2°. The ligand is doubly deprotonated, $\mathbf{L}H_4^{2-}$, with the diazine N2–N3 and N5–N6 distances (1.39(2) Å) indicating single bond character, whereas C–O4 and C–O3 distances are 1.24(1) Å and 1.29(1) Å respectively, reflecting double bond character. These bond distances are similar to those found in complexes of related ligands.[36] Cu1···C2 and Cu1···Cu3 distances are 4.83(2) Å and 4.804(2) Å respectively. N3, N5, O9 and O13 are deprotonated while N1 and N7 are protonated. N1–H is hydrogen bonded to a lattice water (N1···O11 at 2.74(2) Å) whereas N7–H is hydrogen-bonded to a lattice chloride anion (N7···Cl4 at 3.10(1) Å).

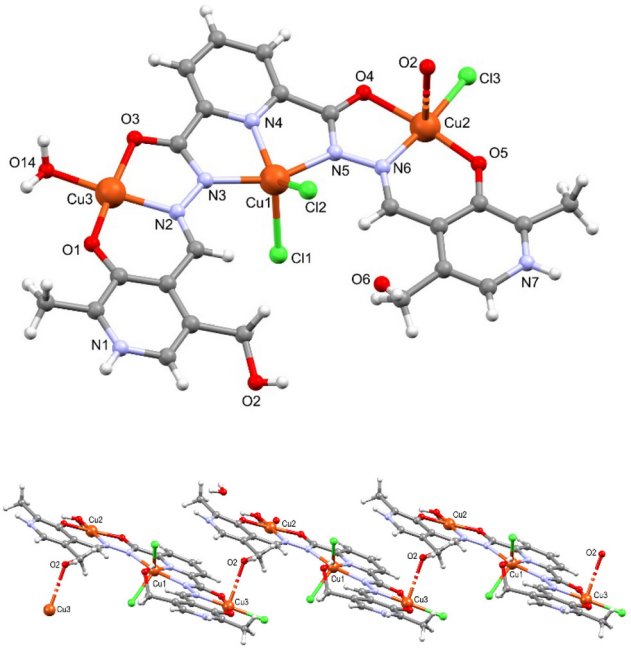

Fig. 1 (top) Molecular structure of $[Cu_3LH_4Cl_3(H_2O)]$ in **1**, (bottom) 1-D polymer chain.

The +6 charge on the three copper(II) ions is balanced by the −4 charge associated with the four crystallographically independent chloride ions (three coordinated and one hydrogen-bonded) and the −2 charge associated with the LH_4^{2-} ligand. The fundamental repeat unit in **1** is a trinuclear $[Cu_3(LH_4)Cl_3(H_2O)]Cl{\cdot}H_2O$ motif (Fig. 1). The trimeric $[Cu_3(LH_4)Cl_3(H_2O)]^+$ units are connected to each other *via* one of the two CH_2OH groups, affording a polymeric 1-D chain topology (Fig. 1). The coordination environment of the Cu3 facilitates polymerization, allowing bridging through CH_2OH groups to generate a one-dimensional polymeric chain (Fig. 1). The Cu1···Cu2 and Cu1···Cu3 separations are 4.830(2) Å, respectively. Additional hydrogen bonds interconnect these 1-D chains to generate a two-dimensional supramolecular arrangement (Fig. S3). Analytical data on a freshly prepared sample were consistent with one coordinated water and four lattice water molecules. This is consistent with the one lattice water identified in the difference map and a void space able to accommodate up to 3.5 additional water molecules (max 4.5 lattice water molecules). TGA data (Fig. S4) revealed a mass loss of 5% upon heating up to 250 °C (dec.), consistent with loss of three lattice waters.

$\{[Cu_3(LH_4)Cl(ClO_4)(H_2O)_2][ClO_4]_2{\cdot}2H_2O\}_n$ (2). Single crystals of the hexameric complex **2**, were obtained by slow evaporation of a methanol/water solution at room temperature. The complex crystallizes in the triclinic space group $P\bar{1}$. Selected bond lengths and angles are provided in Table S3. The asymmetric unit of **2** consists of three Cu(II) ions which are charge-balanced by one LH_4^{2-} ligand, one coordinated chloride ion and three perchlorate anions (one of which is coordinated to Cu3). In addition, there are two coordinated water molecules and two lattice water molecules (Fig. 2). Similar to complex **1**, ligand LH_4^{2-} acts as a tridentate ligand to each of the three crystallographically independent copper ions. Each of the three copper ions in the complex adopts a five-coordinate geometry, with the coordination environment completed by chloride ions (Cu2) or water molecules (Cu1 and Cu3). The central copper ion (Cu1) is coordinated by three nitrogen atoms from the ligand, with the remaining coordination sites occupied by a chloride ion and a water molecule. Like **1**, the geometry around Cu1 is intermediate between trigonal bipyramidal and square pyramidal. In this case, the Addison parameter (τ) of 0.34 for Cu1 is closer to square pyramidal with the chloride ion coordinated in the equatorial plane and an axial water. The peripheral copper ion (Cu3) exhibits a slightly distorted square pyramidal geometry (τ_5 = 0.045). This geometry arises from the coordination of two oxygen atoms and one nitrogen atom from the ligand, along with one water molecule, which collectively constitute the basal plane, while an apical oxygen atom from a perchlorate anion completes the coordination sphere. Cu2 is also 5-coordinate and displays a geometry intermediate between a trigonal bipyramid and a square pyramid (τ_5 = 0.45). As with complex **1**, the central Cu1 ion is connected to the terminal Cu2 and Cu3 ions *via* a *trans* N–N diazine bridge. The Cu1···Cu2 and Cu1···Cu3 separations are 4.831(10) Å and 4.763(1) Å, respectively, which are consistent with those

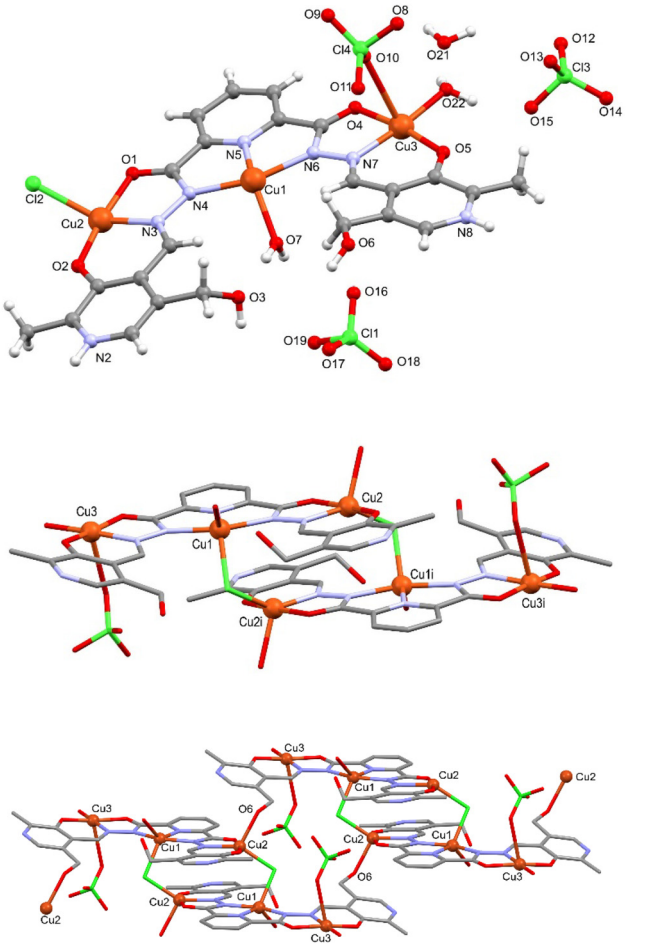

Fig. 2 (top) Asymmetric unit of **2** only the major components of disorder in the ClO_4^- anions are shown for clarity; (centre) dimer of **2** (non-coordinating anions and solvent removed for clarity); (bottom) linking of hexameric units together through coordinate Cu2–O6 bonds. *i* = 1 − *x*, 2 − *y*, 1 − *z*.

observed in other related diazine-bridged complexes.[34] The torsional angles for the Cu2–N6–N7–Cu3 and Cu2–N4–N3–Cu1 bridges are 174.3(3)° and −179.8(3)° respectively, consistent with structures of previously reported diazine complexes.[37] Cu1···C2 and Cu1···Cu3 distances are 4.831(1) Å and 4.763(1) Å respectively. The diazine N3–N4 and N6–N7 bond distances are 1.393(5) Å and 1.388(7) Å, respectively, indicating single-bond character. In contrast, the C4–O1 and C15–O4 distances are 1.263(7) Å and 1.218(6) Å, respectively, consistent with double-bond character.[38] Two trimers are linked together through a pair of Cu1–Cl2–Cu2 links to form a hexamer motif (Fig. 2 middle). These hexameric units are linked *via* coordination of O6 (from a CH_2OH group) to Cu2 of a neighboring molecule, resulting in formation of a one-dimensional polymeric chain. In terms of charge balance, the +6 charge associated with the three Cu(II) ions is counterbalanced by a Cl^- and three ClO_4^- anions as well as the dianionic ligand, LH_4^{2-}. The polymer topology in **1** arises from CH_2OH coordination to Cu,

whereas in **2**, the polymer is generated through a combination of CH_2OH and chloride bridges.

$[Ni_3(LH_4)(H_2O)_9]Cl_4{\cdot}4H_2O$ (3). Dark green single crystals of **3** were obtained from the reaction of $LH_6{\cdot}2HCl$ with $NiCl_2{\cdot}6H_2O$ in methanol. The molecular structure of **3** is illustrated in Fig. 3 and selected interatomic distances and angles are provided in Table S4. The complex crystallizes in the monoclinic space group $P2_1$. The ligand coordinates to three Ni(II) centers in a chain-like arrangement, with Ni1 occupying the central pocket and flanked by two terminal Ni(II) ions, Ni2 and Ni3. All three nickel ions exhibit distorted octahedral coordination geometries. In terms of charge balance the three Ni^{2+} ions are stabilized by four non-coordinating chloride counterions and a LH_4^{2-} ligand. For Ni1, LH_4^{2-} acts as an N_3 donor in the equatorial plane, with Ni–N distances ranging from 2.003(5) Å to 2.169(5) Å with three additional water molecules completing the octahedral geometry with Ni–O distances ranging from 2.041(5) Å to 2.076(5) Å. The peripheral Ni ions (Ni2 and Ni3) also display distorted octahedral geometries. Their equatorial planes consist of one N- and two O-donors derived from LH_4^{2-} and one water molecule, while two additional water molecules complete the primary coordination sphere. The Ni–O distances for Ni2 and Ni3 range from 2.076(6) Å to 2.113(5) Å. Ni1 is connected to Ni2 and Ni3 *via trans* N–N diazine bridges, with torsional angles of Ni2–N1–N5–Ni1 = 174.8(3)° and Ni1–N2–N7–Ni3 = 168.6(3)°. The Ni1···Ni2 separation is 5.035(1) Å, while the Ni1···Ni3 separation is 4.928(1) Å, consistent with other related diazine-bridged complexes.[36] The diazine N–N bond distances (N1–N5 = 1.388(7) Å and N2–N7 = 1.392(8) Å) indicate single-bond character, while the C–O bond distances (C15–O7 = 1.260(7) Å and C16–O2 = 1.254(7) Å) consistent with double-bond character and analogous to both **1** and **2**. These observations are consistent with the deprotonation of the azine N–H group. The nitrogen atoms (N4 and N8) associated with the pyridyl arms remain protonated and do not participate in coordination with the metal ions, instead the pyridinium group is hydrogen bonded to a lattice chloride (N4···Cl1 and N8···Cl2 at 3.070(7) and 3.144(6) Å). Unlike **1** and **2**, the CH_2OH groups remain uncoordinated but are instead involved in hydrogen bonding to a lattice chloride or water (O14···Cl2 at 3.102(7) and O20···O6B at 2.72(1) Å).

$\{[Ni_3(LH_4)(NO_3)(H_2O)_6](NO_3)_3{\cdot}H_2O\}_n$ (4). Dark green single crystals of **4** suitable for X-ray diffraction studies were isolated from the reaction of $LH_6{\cdot}2HCl$ with $Ni(NO_3)_2{\cdot}6H_2O$ in methanol. The molecular structure of **4** is shown in Fig. 4, and selected interatomic distances and angles are listed in Table S5. The complex crystallizes in the monoclinic space group $P\bar{1}$. All three nickel ions in the asymmetric unit are six coordinate. The +6 charge associated with the three Ni(II) ions in the trinuclear repeat unit is balanced by the presence of four nitrate ions and an overall charge of −2 on the ligand, LH_4^{2-}. The LH_4^{2-} ligand binds three nickel ions in an analogous fashion to the binding of copper and nickel ions in complexes **1–3**. The central nickel ion (Ni1) is six-coordinate, with an NiN_3O_3 coordination geometry, comprising three nitrogen donors from LH_4^{2-}, two oxygen atoms from a chelating nitrate anion and one water ligand. The terminal nickel ion (Ni2) adopts a $NiNO_5$ coordination geometry, comprising an NO_2 donor set from LH_4^{2-} with the coordination sphere completed by three water molecules. Ni3 also adopts a $NiNO_5$ coordination geometry with LH_4^{2-} again providing an NO_2 donor set with the remaining coordination sites comprising two water molecules and a pendant O3 atom from a symmetry-related CH_2OH group ($1 + x, y, z$). The latter generates a one-dimensional polymer which propagates along the crystallographic

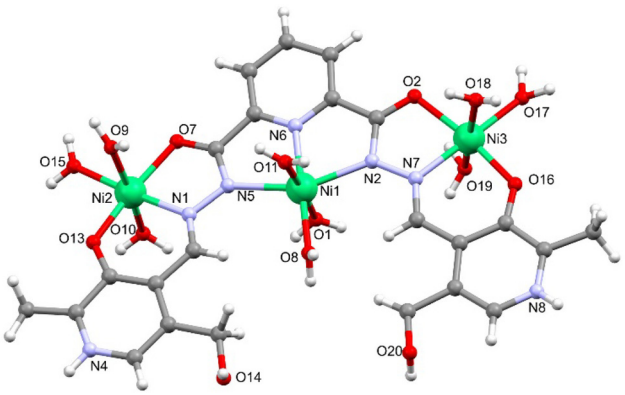

Fig. 3 Molecular structure of $[Ni_3(L)(H_2O)_9]$ in **3**.

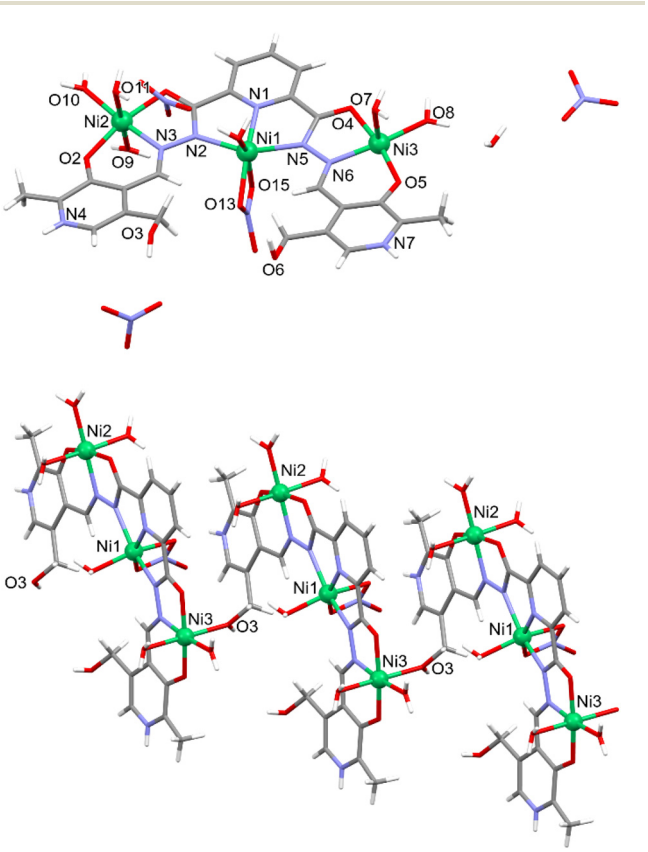

Fig. 4 (top) Asymmetric unit of **4**. (bottom) 1-D polymer chain of **4**.

a-axis (Fig. 4). The pyridinium groups form a bifurcated hydrogen bond N7···O22/N7···O24 to a lattice nitrate anion (N···O 3.032(7) and 2.979(7) Å respectively) and a hydrogen bond N4···O15 to the coordinated nitrate (N···O 2.651(6) Å). The Ni1···Ni2 separation is 4.938(9) Å, while the Ni1···Ni3 separation is 4.955(9) Å,

$[Ni_2(LH_6)(H_2O)_6](ClO_4)_4{\cdot}3H_2O$ (5). When the reaction of $LH_6{\cdot}2HCl$ with $Ni(ClO_4)_2{\cdot}6H_2O$ is performed in methanol, crystals of **5** are isolated by slow evaporation of the mother liquor. This complex crystallizes in the triclinic space group $P\bar{1}$. The molecular structure of **5** is shown in Fig. 5 and selected interatomic distances and angles are listed in Table S6. In contrast to complexes **1–4**, the ligand in complex **5** binds to only two Ni(II) ions *via* the peripheral NO_2 donor sets while, unexpectedly, the central N_3-donor pocket does not coordinate a metal ion. Instead, it is occupied by two perchlorate anions, which are hydrogen bonded to the hydrazone protons (Fig. 5 bottom). With regard to charge balance, the two Ni(II) ions are balanced by four non-coordinated ClO_4^- anions and the ligand is bound in the formally neutral LH_6 form in which the two diazine groups remain protonated. The coordination environments around Ni1 and Ni2 are very similar to Ni1 and Ni3 in complex **3**, *i.e.* both exhibit a $NiNO_5$ coordination environment with LH_6 acting as an NO_2 donor and the remaining three coordination sites occupied by water molecules. The terminal oxygen atoms O3 and O6 form hydrogen bonds with their symmetry equivalents (O3i and O6i), resulting in a hydrogen-bonded dimeric unit. Although formally charge neutral the LH_6 ligand exists in a zwitterionic form where the phenolic OH (associated with O2 and O5) undergo tautomerization with their protons associated with the pyridinium groups. The pyridinium groups are hydrogen bonded to a ClO_4^- anion and a lattice water. The Ni1···Ni2 separation is 10.030(1) Å.

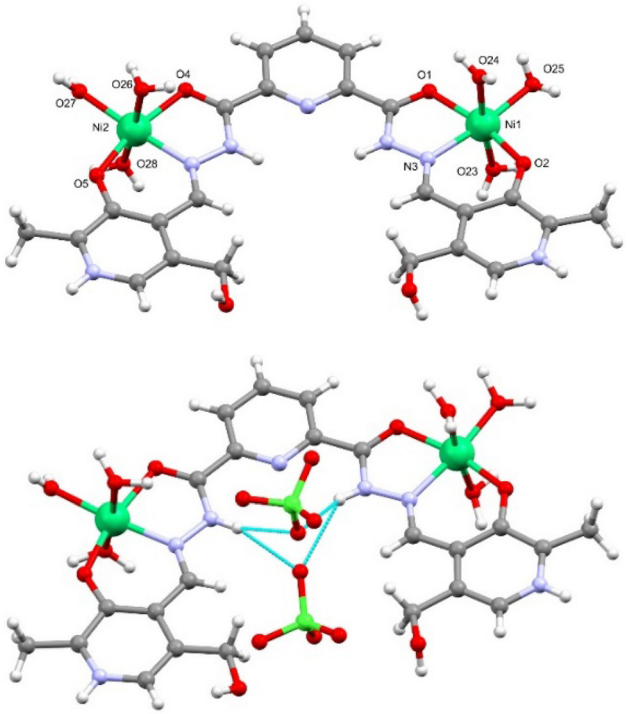

Fig. 5 (top) Molecular structure of the $[Ni_2(LH_6)(H_2O)_6]^{4+}$ cation in **5** (four charge balancing ClO_4^- anions and lattice solvent omitted for clarity); (bottom). Interaction of two ClO_4^- anions with the structure of $[Ni_2(L)(H_2O)_6]^{4+}$.

Comparison of complexes 1–5

Complexes **1–4** all possess a common $[M_3(LH_4)]^{4+}$ core. In **1**, three of the four Cl^- anions are coordinated (two to the central Cu1 and one to the peripheral Cu2), whereas in **2** one Cl^- and one ClO_4^- anion are coordinated to peripheral Cu2 and Cu3 ions respectively. In the case of the nickel complexes, there is less association of anions with the $[M_3(\mathbf{LH_4})]^{4+}$ and $[M_2(\mathbf{LH_6})]^{4+}$ cations in **3** and **5**, both of which complete their coordination environments with water molecules.

Only in **4** is one of the charge-balancing counterions coordinated, with NO_3^- coordinated to the central Ni1 ion. Attempts to make the corresponding Cu(I) complex with nitrate anions by using Cu(II) nitrate as the precursor were unsuccessful, forming only oily residues. In all structures, the phenolic proton is transferred to the pyridine moiety, increasing the donor capacity of the O to participate in chelating the metal, while the resultant pyridinium group is invariably involved in hydrogen bonding to anions or lattice water. The alcoholic CH_2OH pendant arm takes a key role in the supramolecular structures of several these complexes: In **1**, **2** and **4**, the ability of one of the CH_2OH groups to bridge affords polymeric chain motifs. In **5**, the CH_2OH groups are involved in hydrogen bonding.

Magnetic properties of complexes

DC magnetic data on complexes **1–3** were recorded on a Quantum Design SQUID magnetometer using an applied field of 0.3 T across the temperature range 2–300 K. The geometry of the trinuclear core **4** is very similar to **5** and the magnetism of **5** recorded as representative of this spin topology. For **5** the DC magnetic data were recorded in a DC field of 0.2 T. Samples (17.6–30.0 mg) were mounted in gelatin capsules and corrections were applied for sample diamagnetism. Modelling of all data was undertaken in PHI.[39]

The structure of **1** reveals an asymmetric unit comprising a trimetallic $\{Cu_3\}$ unit, linked together *via* coordinate bonds from the CH_2OH group. Since this linker comprises a 6-atom bridge containing some saturated C atoms, then superexchange between trimer building blocks was neglected and the magnetic data were modelled as a symmetric trimer in which there are two *trans* μ-N_2-bridges. A plot of $1/\chi$ *vs.* T for the trimer in the high temperature range (100–300 K, Fig. S8) reveals a Curie constant, C = 1.37 cm^3 K mol^{-1}, close to the value expected for three independent $S = \frac{1}{2}$ Cu^{2+} ions with g = 2.21 (C = 1.37 cm^3 K mol^{-1}). The Weiss constant, θ, is −112 K, consistent with the presence of dominant antiferromagnetic interactions. Although the two μ-N_2 linkers between Cu^{2+} ions are crystalographically independent, the conformations are

very similar and the temperature dependence of χT was modelled using the Hamiltonian:

$$\hat{H} = -2J[\hat{S}_1\hat{S}_2 + \hat{S}_2\hat{S}_3] \quad (1)$$

A two-parameter fit (g and J) reflected the temperature dependence of χT across the range 3–300 K with g = 2.140 (±0.006) and J = −62(±1) cm^{-1}. Below 50 K, a plateau in χT at 0.44 cm^3 K mol^{-1} is evident, consistent with an $S_T = \frac{1}{2}$ ground state (g = 2.17), expected for antiferromagnetic exchange in a linear $S = \frac{1}{2}$ trimer.

For **2**, the crystal structure reveals a similar asymmetric unit to **1**, comprising a trimetallic {Cu$_3$} unit. However, in the case of **2**, two trimers are linked *via* two bridging μ-Cl bridges to form hexamers. A schematic of the spin topology and exchange pathways is shown in Fig. 6 (inset). Although these hexamers are further linked through bridging CH$_2$OH groups to form a polymeric network, similar arguments can be made (as for **1**) that the 6-atom bridge between Cu(II) ions can be neglected as a significant exchange pathway. As a consequence the magnetic data observed for **2** were modelled as a hexamer in which there are *trans*-μ-N$_2$ bridges and a pair of symmetry equivalent μ-Cl bridges. A plot of $1/\chi$ *vs.* T for the hexameric unit in the high temperature range (100–300 K, Fig. S-9) reveals a Curie constant, C = 2.73 cm^3 K mol^{-1}, close to the value expected for six $S = \frac{1}{2}$ Cu^{2+} ions with g = 2.2 (C = 2.72 cm^3 K mol^{-1}) and similar to the g-value for complex **1**. The Weiss constant, θ, is −113 K, consistent with the presence of dominant antiferromagnetic interactions and almost identical to that observed for **1**. Given the similarity in the two crystallographically independent μ-N$_2$ linkers between Cu^{2+} ions, the temperature dependence of χT was modelled using the Hamiltonian:

$$\hat{H} = -2J_1[\hat{S}_1\hat{S}_2 + \hat{S}_2\hat{S}_3 + \hat{S}_4\hat{S}_5 + \hat{S}_5\hat{S}_6] - 2J_2[\hat{S}_2\hat{S}_4 + \hat{S}_3\hat{S}_5] \quad (2)$$

where J_1 corresponds to exchange *via* the μ-N$_2$ bridge and J_2 reflects exchange *via* the μ-Cl. A three-parameter fit (g, J_1 and J_2) replicated the temperature dependence of χT across the range 5–300 K with g = 2.069(±0.006), J_1 = −53.7(±0.8) cm^{-1} and J_2 = +3.7(±0.1) cm^{-1}. The values of J_1 is in gratifying agreement with the value of J found for **1** (−62 ± 1 cm^{-1}) for the same diazine bridge exchange pathway. The dominant antiferromagnetic exchange *via* the μ-N$_2$ bridges leads to a decrease in χT upon coolin down to *ca.* 0.8 cm^3 K mol^{-1} at 50 K (twice the value of the trimer **1**), before decreasing again upon further cooling. This might initially seem unexpected given the ferromagnetic nature of J_2 but a plot of the spin arrangement using antiferromagnetic J_1 and ferromagnetic J_2 shows that an S_T = 0 ground term is expected (Fig. 6, inset).

The magnetic orbitals in the basal plane facilitates efficient exchange coupling through the *trans*-diazine unit. Previous studies on diazine systems indicate a linear relationship between the exchange coupling and the rotational angle of Cu magnetic planes relative to the single N–N bond.[37] Cu–N–N–Cu torsion angles (α, α′) and bond angles (β, β′) in **1** and **2** in the range 174.30°–179.80° and 108.4°–119° respectively which are quite close to the related examples leading to strong antiferromagnetic interactions.[36,40,41]

For the Ni trimer (**3**), a plot of $1/\chi$ *vs.* T in the high temperature range (100–300 K, Fig. S10) reveals a Curie constant, C = 2.92 cm^3 K mol^{-1}, close to the value expected for three S = 1 Ni^{2+} ions with g = 2.0 (C = 3.00 cm^3 K mol^{-1}). The Weiss constant, θ, is −10.6 K, consistent with the presence of dominant antiferromagnetic interactions, although a contribution from zero field splitting cannot be discounted. As with 1, the two μ-N$_2$ linkers between Ni^{2+} ions are crystallographically independent but both exhibit similar conformations. As a consequence, the temperature dependence of χT was fitted to eqn (1) (Fig. 7). A two-parameter fit (g and J) replicated the temperature dependence of χT across the range 5–300 K with g = 2.092(±0.007) and J = −6.6(±0.2) cm^{-1}. The antiferromagnetic coupling between Ni^{2+} ions affords an S_T = 1 ground term. In nickel complexes with small Ni–N–N–Ni torsional angles, no significant magnetic interaction is observed.[42] In contrast, complexes with large torsional angles (~160°) exhibit weak to moderate antiferromagnetic coupling[43,44] consistent with the behaviour observed for compound **3**.

For the dimeric Ni(II) complex (**5**), there is no efficient magnetic exchange pathway (7 atom bridge) and so magnetic exchange is likely weak and zero field splitting of the single ions may be dominant. A plot of $1/\chi$ *vs.* T for the trimer in the

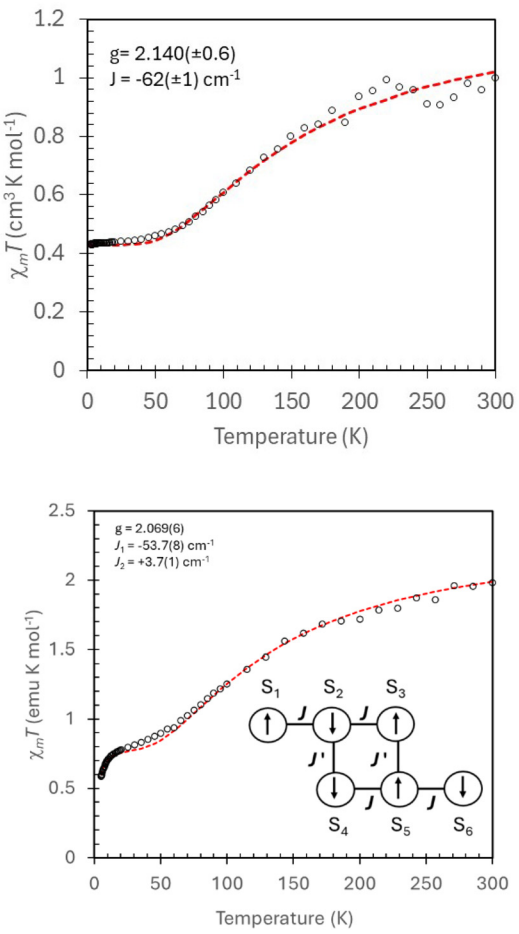

Fig. 6 Temperature dependence of χT for **1** (top) and **2** (bottom).

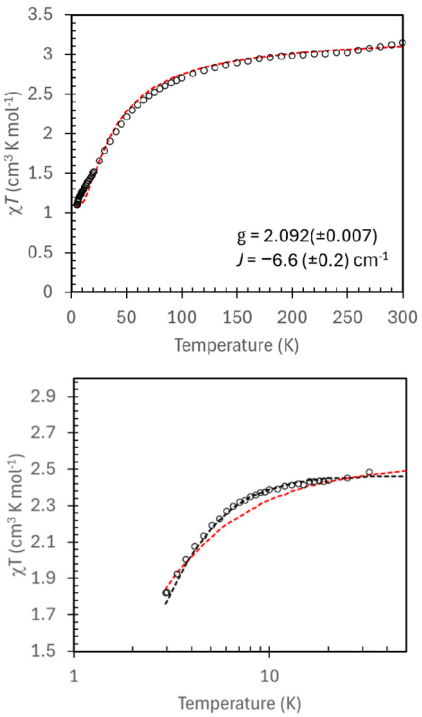

Fig. 7 Temperature dependence of χT for **3** (top) and **5** (bottom). For **3**, the red line corresponds to the best fit to the experimental data according to eqn (1). For **5**, the dashed red line corresponds to the best fit to eqn (1), whereas the dashed black line represents the effect of an axial zero field splitting.

high temperature range (100–300 K, Fig. S11) reveals a Curie constant, C = 2.82 cm^3 K mol^{-1}, close to the value expected for two S = 1 Ni^{2+} ions with g = 2.37 (C = 2.81 cm^3 K mol^{-1}) and a Weiss constant, θ = −9.6 K. A fit to an exchange-coupled dimer using the Hamiltonian:

$$\hat{H} = -2J[\hat{S}_1\hat{S}_2] \quad (3)$$

afforded g = 2.249(±0.007) and J = −0.40(±0.02) cm^{-1}. However, given the absence of an efficient exchange pathway between Ni(II) ions, it is feasible that the downturn in χT at low temperature could be due to zero field splitting of the S = 1 Ni(II) ion in octahedral coordination. Taking the two Ni(II) ions as having the same geometry and ZFS parameters, an improved fit to the data was also observed with g = 2.220(±0.007) and D = 1.66 ± 0.07 cm^{-1} (Fig. 7 bottom). Of the two models, the single ion model with zero field splitting appears the better fit. Although a combination of both exchange and zero field splitting (ZFS) effects are feasible, the reasonable fit with the ZFS model alone means that including both terms would lead to overparameterization. The ZFS parameter D is comparable to other octahedral nickel(II) complexes.[45]

Discussion

The complexes **1–4** all exhibit a common trimetallic sub-unit, $[M_3LH_4]^{4+}$ with the remaining coordination sites occupied by

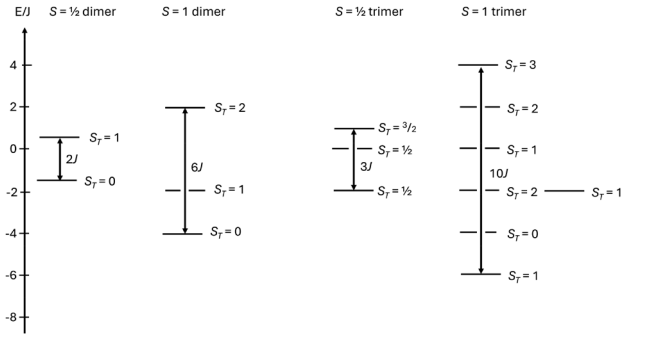

Fig. 8 Spin states arising for magnetic exchange in (left) $S = \frac{1}{2}$ and S = 1 dimers (right), $S = \frac{1}{2}$ and S = 1 trimers.

counterions, solvent or the CH_2OH group of another LH_4^{2-} ligand. The magnetic measurements clearly reveal strong antiferromagnetic exchange between Cu ions in both the trimetallic complex **1** and hexameric **2** with J = −62 and −54 cm^{-1} respectively. For **1** and **2**, the Jahn–Teller elongation leads to both Cu^{2+} ions possessing a magnetic orbital of $d_{x_2-y_2}$ character, each capable of σ-delocalization to the diazine bridge, leading to a lack of orbital orthogonality and antiferromagnetic exchange between these ions. Similar arguments can be made for **3**, with a smaller exchange coupling, J = −6.6 cm^{-1}. The decrease in J is largely associated with the increase in spin quantum number, S, with metal complexes possessing larger values of S leading to smaller values of J. For example, solution of the spin Hamiltonian for a dimer eqn (3) affords two spin states for a copper(II) dimer corresponding to S_T = 0 and S_T = 1, separated by an energy term 2J (Fig. 8). For a nickel(II) dimer, exchange coupling affords S_T = 2, S_T = 1 and S_T = 0 states. In this latter case, the separation of the ferromagnetically aligned spin orientation (S_T = 2) and the antiferromagnetic spin orientation (S_T = 0) is now 6J. The energy difference between ferromagnetic and antiferromagnetic spin orientations for copper is 2J, but 6J for nickel. If we are considering J in terms of the energetic difference between coparallel and antiparallel spin alignments, then J for nickel would be 1/3 of the value of J for copper. For a linear trimer, the system is more complex, the energy difference between idealized "↑↑↑" and "↑↓↑" configurations are 3J for copper and 10J for Ni. A plot of the spin states for the copper trimer and nickel trimer are shown in Fig. 8. The energy difference between the $S = \frac{1}{2}$ and the $S = \frac{3}{2}$ states for the copper trimer **1** is 186 cm^{-1} whereas it is 66 cm^{-1} for the nickel trimer **3**. In real terms the exchange coupling is weaker in the nickel system.

Conclusions

In the present study, we successfully synthesized nickel and copper complexes using a new polydentate open chain diazine-based ligand LH_6 that incorporate different N-and O-donor coordination pockets. All of the coordination pockets of the ligand were occupied with metals when reacted with metal

salts except in the case of **5** where the central *NN′N″* pocket remains empty and may be due to the presence of two perchlorate anions which are involved in hydrogen-bonding to the hydrazone protons blocking the entry of third metal. In complexes **1**, **2**, **3** and **4**, the d-block metal ions are all linked *trans via* the two-atom diazine bridge. Magnetic studies reveal the presence of strong antiferromagnetic interactions in **1** with $J = -62$ cm^{-1} (**1**) giving rise to an $S_T = \frac{1}{2}$ ground state, whereas in **2**, the additional exchange pathways *via* the μ-Cl result in an $S_T = 0$ ground term due to weak ferromagnetic coupling between trimer units. Complex **3** also exhibits antiferromagnetic exchange interactions *via* the diazine bridge with $J = -6.6(\pm 0.2)$ cm^{-1}. For complex **5**, there is no efficient exchange pathway between the two Ni(II) ions and the magnetic data were reproduced using an axial zero field splitting ($D = 1.66 \pm 0.07$ cm^{-1}). This work bridges three critical gaps in molecular magnetism. (i) It introduces pyridoxal–diazine hybrids as a new ligand class for polynuclear complexes. (ii) It provides the first systematic comparison of magnetic coupling in isostructural Cu *vs.* Ni clusters, revealing metal-specific trends. (iii) It demonstrates how ligand rigidity (diazine) and flexibility (pyridoxal chelation) can coexist to stabilize extended architectures. These findings open avenues for designing stimuli-responsive magnetic materials, where pyridoxal's redox activity could enable external control over spin states. Future studies will explore further ligand modifications to modulate exchange interactions and probe magneto-structural correlations in higher-dimensional networks.

Conflicts of interest

There are no conflicts to declare.

Data availability

Supplementary information (SI) is available. See DOI: https://doi.org/10.1039/d5dt02226f.

CCDC 2488451–2488455 contain the supplementary crystallographic data for this paper.[46a–e]

Acknowledgements

MUA thank MOHERI (BFP/RGP/CBS/24/221 (https://rims.trc.gov.om/converis/mypages/browse/Project application/68573034)) and the University of Nizwa for financial support. J. M. R. and M. P. thank NSERC for operating (DG-2020-04627 and DG-2018-04255 respectively) and infrastructure grants (J. M. R., RTI-2022-00005).

References

1 R. Alotaibi, A. Booth, E. Little, A. Brookfield, A. Achari, S. J. Lockyer, G. A. Timco, G. F. S. Whitehead, I. J. Vitórica-Yrezábal and N. F. Chilton, *Dalton Trans.*, 2023, **52**, 7473–7481.
2 J. A. Davies, *Synthetic coordination chemistry: principles and practice*, World Scientific, 1996.
3 Y. B. Go, X. Wang, E. V. Anokhina and A. J. Jacobson, *Inorg. Chem.*, 2005, **44**, 8265–8271.
4 Z. Xu, L. K. Thompson and D. O. Miller, *Inorg. Chem.*, 1997, **36**, 3985–3995.
5 L. N. Dawe, T. S. M. Abedin and L. K. Thompson, *Dalton Trans.*, 2008, 1661–1675.
6 C. J. Elsevier, J. Reedijk, P. H. Walton and M. D. Ward, *Dalton Trans.*, 2003, 1869–1880.
7 L. N. Dawe, K. V. Shuvaev and L. K. Thompson, *Chem. Soc. Rev.*, 2009, **38**, 2334–2359.
8 C. J. Matthews, L. K. Thompson, S. R. Parsons, Z. Xu, D. O. Miller and S. L. Heath, *Inorg. Chem.*, 2001, **40**, 4448–4454.
9 A. Stadler, N. Kyritsakas, R. Graff and J. Lehn, *Chem. – Eur. J.*, 2006, **12**, 4503–4522.
10 R. E. P. Winpenny, *J. Chem. Soc., Dalton Trans.*, 2002, 1–10.
11 A. Garau, G. Picci, M. Arca, A. J. Blake, C. Caltagirone, G. De Filippo, F. Demartin, F. Isaia, V. Lippolis and A. Pintus, *Molecules*, 2021, **26**, 1286.
12 R. W. Saalfrank, E. Uller, B. Demleitner and I. Bernt, *Mol. Self-Assembly Org. Versus Inorg. Approaches*, 2000, pp. 149–175.
13 M. U. Anwar, L. N. Dawe, M. S. Alam and L. K. Thompson, *Inorg. Chem.*, 2012, **51**, 11241–11250.
14 G. Christou, D. Gatteschi, D. N. Hendrickson and R. Sessoli, *MRS Bull.*, 2000, **25**, 66–71.
15 M. U. Anwar, A. Al-Harrasi, J. M. Rawson, E. L. Gavey, J. Regier, D. Alexandropoulos, M. Pilkington and L. K. Thompson, *Dalton Trans.*, 2019, **48**, 14269–14278.
16 M. M. Turnbull, C. P. Landee and B. M. Wells, *Coord. Chem. Rev.*, 2005, **249**, 2567–2576.
17 G. A. Craig, A. Sarkar, C. H. Woodall, M. A. Hay, K. E. R. Marriott, K. V. Kamenev, S. A. Moggach, E. K. Brechin, S. Parsons and G. Rajaraman, *Chem. Sci.*, 2018, **9**, 1551–1559.
18 R. T. Butcher, L. N. Dawe, C. P. Landee and M. M. Turnbull, *Polyhedron*, 2009, **28**, 1710–1713.
19 J. Bartolomé, E. Bartolomé, F. Luis, E. Burzurí, A. Camón, G. Filoti, A. M. Ako, J. Braun, V. Mereacre and C. E. Anson, *Inorg. Chem.*, 2024, **63**, 24262–24273.
20 A. Hussain, K. Mariappan, D. C. Cork, L. D. Lewandowski, P. K. Shrestha, S. Giri, X. Wang and A. G. Sykes, *RSC Adv.*, 2021, **11**, 34181–34192.
21 A. Karim, S. Ullah, S. A. Halim, W. Ali, A. Khan, A. Al-Harrasi and M. U. Anwar, *Appl. Organomet. Chem.*, 2025, **39**, e70024.
22 M. U. Anwar, L. N. Dawe, S. R. Parsons, S. S. Tandon, L. K. Thompson, S. K. Dey, V. Mereacre, W. M. Reiff and S. D. Bunge, *Inorg. Chem.*, 2014, **53**, 4655–4668.
23 M. U. Anwar, S. S. Tandon, L. N. Dawe, F. Habib, M. Murugesu and L. K. Thompson, *Inorg. Chem.*, 2012, **51**, 1028–1034.

24 V. A. Milway, L. Zhao, T. S. M. Abedin, L. K. Thompson and Z. Xu, *Polyhedron*, 2003, **22**, 1271–1279.
25 A. X. S. Bruker and V. Saint-plus, *Acta Crystallogr., Sect. A: Found. Crystallogr.*, 1995, **51**, 33.
26 L. Krause, R. Herbst-Irmer, G. M. Sheldrick and D. Stalke, *Appl. Crystallogr.*, 2015, **48**, 3–10.
27 G. M. Sheldrick, *Acta Crystallogr., Sect. A:Found. Adv.*, 2015, **71**, 3–8.
28 G. M. Sheldrick, *Acta Crystallogr., Sect. C:Struct. Chem.*, 2015, **71**, 3–8.
29 C. R. Groom, I. J. Bruno, M. P. Lightfoot and S. C. Ward, *Struct. Sci.*, 2016, **72**, 171–179.
30 D. Kratzert and I. Krossing, *J. Appl. Crystallogr.*, 2019, **52**, 468–471.
31 T. Mukherjee, J. C. Pessoa, A. Kumar and A. R. Sarkar, *Inorg. Chim. Acta*, 2015, **426**, 150–159.
32 A. Brisdon, *Appl. Organomet. Chem.*, 2010, **24**, 489.
33 A. W. Addison, T. N. Rao, J. Reedijk, J. van Rijn and G. C. Verschoor, *J. Chem. Soc., Dalton Trans.*, 1984, 1349–1356.
34 M. U. Anwar, L. K. Thompson and L. N. Dawe, *Dalton Trans.*, 2011, **40**, 1437–1440.
35 B. Cordero, V. Gómez, A. E. Platero-Prats, M. Revés, J. Echeverría, E. Cremades, F. Barragán and S. Alvarez, *Dalton Trans.*, 2008, 2832–2838.
36 M. U. Anwar, A. Al-Harrasi, E. L. Gavey, M. Pilkington, J. M. Rawson and L. K. Thompson, *Dalton Trans.*, 2018, **47**, 2511–2521.
37 M. U. Anwar, J. M. Rawson, E. L. Gavey, M. Pilkington, A. Al-Harrasi and L. K. Thompson, *Dalton Trans.*, 2017, **46**, 2105–2113.
38 J. M. Rawson and R. E. P. Winpenny, *Coord. Chem. Rev.*, 1995, **139**, 313–374.
39 N. F. Chilton, R. P. Anderson, L. D. Turner, A. Soncini and K. S. Murray, *J. Comput. Chem.*, 2013, **34**, 1164–1175.
40 V. A. Milway, V. Niel, T. S. M. Abedin, Z. Xu, L. K. Thompson, H. Grove, D. O. Miller and S. R. Parsons, *Inorg. Chem.*, 2004, **43**, 1874–1884.
41 L. K. Thompson, Z. Xu, A. E. Goeta, J. A. K. Howard, H. J. Clase and D. O. Miller, *Inorg. Chem.*, 1998, **37**, 3217–3229.
42 Z. Xu, L. K. Thompson, D. O. Miller, H. J. Clase, J. A. K. Howard and A. E. Goeta, *Inorg. Chem.*, 1998, **37**, 3620–3627.
43 Z. Xu, L. K. Thompson, V. A. Milway, L. Zhao, T. Kelly and D. O. Miller, *Inorg. Chem.*, 2003, **42**, 2950–2959.
44 Z. Xu, L. K. Thompson, D. A. Black, C. Ralph, D. O. Miller, M. A. Leech and J. A. K. Howard, *J. Chem. Soc., Dalton Trans.*, 2001, 2042–2048.
45 H. Sakiyama, R. Kimura, H. Oomiya, R. Mitsuhashi, S. Fujii, K. Kanaizuka, M. Muddassir, Y. Tamaki, E. Asato and M. Handa, *Magnetochemistry*, 2024, **10**, 32.
46 (*a*) CCDC 2488451: Experimental Crystal Structure Determination, 2025, DOI: 10.5517/ccdc.csd.cc2pjfm9; (*b*) CCDC 2488452: Experimental Crystal Structure Determination, 2025, DOI: 10.5517/ccdc.csd.cc2pjfnb; (*c*) CCDC 2488453: Experimental Crystal Structure Determination, 2025, DOI: 10.5517/ccdc.csd.cc2pjfpc; (*d*) CCDC 2488454: Experimental Crystal Structure Determination, 2025, DOI: 10.5517/ccdc.csd.cc2pjfqd; (*e*) CCDC 2488455: Experimental Crystal Structure Determination, 2025, DOI: 10.5517/ccdc.csd.cc2pjfrf.